Chinese Physical Society | IOP Publishing
CPB
Chinese Physics B
http://cpb.iphy.ac.cn https://iopscience.iop.org/journal/1674-1056

Enhancement of spin-orbit torque efficiency by tailoring interfacial spin-orbit coupling in Pt-based magnetic multilayers

Wenqiang Wang(王文强), Gengkuan Zhu(朱耿宽), Kaiyuan Zhou(周恺元), Xiang Zhan(战翔), Zui Tao(陶醉), Qingwei Fu(付清为), Like Liang(梁力克), Zishuang Li(李子爽), Lina Chen(陈丽娜), Chunjie Yan(晏春杰), Haotian Li(李浩天), Tiejun Zhou(周铁军), and Ronghua Liu(刘荣华)

Citation: Chin. Phys. B, 2022, 31 (**9**): 097504. DOI: 10.1088/1674-1056/ac76aa
Journal homepage: http://cpb.iphy.ac.cn; http://iopscience.iop.org/cpb

What follows is a list of articles you may be interested in

Probing the magnetization switching with in-plane magnetic anisotropy through field-modified magnetoresistance measurement

Runrun Hao(郝润润), Kun Zhang(张昆), Yinggang Li(李迎港), Qiang Cao(曹强), Xueying Zhang(张学莹), Dapeng Zhu(朱大鹏), and Weisheng Zhao(赵巍胜)

Chin. Phys. B, 2022, 31 (**1**): 017502. DOI: 10.1088/1674-1056/ac21bb

Spin orbit torques in Pt-based heterostructures with van der Waals interface

Qian Chen(陈倩), Weiming Lv(吕伟明), Shangkun Li(李尚坤), Wenxing Lv(吕文星), Jialin Cai(蔡佳林), Yonghui Zhu(朱永慧), Jiachen Wang(王佳晨), Rongxin Li(李荣鑫), Baoshun Zhang(张宝顺), and Zhongming Zeng(曾中明)

Chin. Phys. B, 2021, 30 (**9**): 097506. DOI: 10.1088/1674-1056/ac0908

Enhanced spin-orbit torque efficiency in $Pt_{100-x}Ni_x$ alloy based magnetic bilayer

Congli He(何聪丽), Qingqiang Chen(陈庆强), Shipeng Shen(申世鹏), Jinwu Wei(魏晋武), Hongjun Xu(许洪军), Yunchi Zhao(赵云驰), Guoqiang Yu(于国强), and Shouguo Wang(王守国)

Chin. Phys. B, 2021, 30 (**3**): 037503. DOI: 10.1088/1674-1056/abe3f4

Magnetization reorientation induced by spin–orbit torque in YIG/Pt bilayers

Ying-Yi Tian(田颖异), Shuan-Hu Wang(王拴虎), Gang Li(李刚), Hao Li(李豪), Shu-Qin Li(李书琴), Yang Zhao(赵阳), Xiao-Min Cui(崔晓敏), Jian-Yuan Wang(王建元), Lv-Kuan Zou(邹吕宽), and Ke-Xin Jin(金克新)

Chin. Phys. B, 2020, 29 (**11**): 117504. DOI: 10.1088/1674-1056/abb666

Electrical transport and optical properties of Cd_3As_2 thin films

Yun-Kun Yang(杨运坤), Fa-Xian Xiu(修发贤), Feng-Qiu Wang(王枫秋), Jun Wang(王军), Yi Shi(施毅)

Chin. Phys. B, 2019, 28 (**10**): 107502. DOI: 10.1088/1674-1056/ab3a91

Chin. Phys. B **31**, 097504 (2022)

RAPID COMMUNICATION

Enhancement of spin–orbit torque efficiency by tailoring interfacial spin–orbit coupling in Pt-based magnetic multilayers

Wenqiang Wang(王文强)[1], Gengkuan Zhu(朱耿宽)[1], Kaiyuan Zhou(周恺元)[1], Xiang Zhan(战翔)[1], Zui Tao(陶醉)[1], Qingwei Fu(付清为)[1], Like Liang(梁力克)[1], Zishuang Li(李子爽)[1], Lina Chen(陈丽娜)[1,2,†], Chunjie Yan(晏春杰)[1], Haotian Li(李浩天)[1], Tiejun Zhou(周铁军)[3,‡], and Ronghua Liu(刘荣华)[1,§]

[1] *National Laboratory of Solid State Microstructures, School of Physics and Collaborative Innovation Center of Advanced Microstructures, Nanjing University, Nanjing* 210093, *China*

[2] *New Energy Technology Engineering Laboratory of Jiangsu Provence and School of Science, Nanjing University of Posts and Telecommunications, Nanjing* 210023, *China*

[3] *Centre for Integrated Spintronic Devices, School of Electronics and Information, Hangzhou Dianzi University, Hangzhou* 310018, *China*

(Received 6 April 2022; revised manuscript received 28 May 2022; accepted manuscript online 8 June 2022)

We study inserting Co layer thickness-dependent spin transport and spin–orbit torques (SOTs) in the Pt/Co/Py trilayers by spin-torque ferromagnetic resonance. The interfacial perpendicular magnetic anisotropy (IPMA) energy density (K_s = 2.7 erg/cm^2, 1 erg = 10^{-7} J), which is dominated by interfacial spin–orbit coupling (ISOC) in the Pt/Co interface, total effective spin-mixing conductance ($G^{\uparrow\downarrow}_{\text{eff,tot}} = 0.42\times10^{15}\ \Omega^{-1}\cdot\text{m}^{-2}$) and two-magnon scattering ($\beta_{\text{TMS}} = 0.46$ nm^2) are first characterized, and the damping-like torque ($\xi_{\text{DL}} = 0.103$) and field-like torque ($\xi_{\text{FL}} = -0.017$) efficiencies are also calculated quantitatively by varying the thickness of the inserting Co layer. The significant enhancement of ξ_{DL} and ξ_{FL} in Pt/Co/Py than Pt/Py bilayer system originates from the interfacial Rashba–Edelstein effect due to the strong ISOC between Co-3d and Pt-5d orbitals at the Pt/Co interface. Additionally, we find a considerable out-of-plane spin polarization SOT, which is ascribed to the spin anomalous Hall effect and possible spin precession effect due to IPMA-induced perpendicular magnetization at the Pt/Co interface. Our results demonstrate that the ISOC of the Pt/Co interface plays a vital role in spin transport and SOTs-generation. Our finds offer an alternative approach to improve the conventional SOTs efficiencies and generate unconventional SOTs with out-of-plane spin polarization to develop low power Pt-based spintronic via tailoring the Pt/FM interface.

Keywords: spin–orbit torque, interfacial Rashba–Edelstein effect, spin-torque efficiency, spin-torque ferromagnetic resonance

PACS: 75.70.Tj, 75.70.–i, 75.76.+j, 75.78.–n **DOI:** 10.1088/1674-1056/ac76aa

1. Introduction

Spin–orbit torques (SOTs)[1–8] in heavy metal/ferromagnet (HM/FM) systems have become a powerful approach to achieving a pure current control of magnetization switch for building an energy-efficient SOT-magnetoresistive random-access memory (SOT-MRAM)[9] and excitation of coherent spin waves for magnon-based logic devices[10,11] or spin synchronization-based neuromorphic computing.[12–14]

The generation of SOTs originates from the orbital angular momentum transferred from the lattice to the spin system due to the spin–orbit interaction in the HM with strong bulk spin–orbit coupling (SOC) or/and at the HM/FM interface with strong interfacial spin–orbit coupling (ISOC). The former is generally described as the spin Hall effect (SHE), and the latter is commonly known as the interfacial Rashba–Edelstein effect (IREE).[15] As shown in Fig. 1(a), SHE/IREE-generated in-plane (IP) transverse polarization $\boldsymbol{\sigma}_y$ spin currents exert two types of SOTs on the magnetization $\boldsymbol{m}$ of the adjacent FM layer: one is the IP damping-like (DL) torque[1,16] $\tau_{\text{DL}} = \tau_{\text{DL}}\boldsymbol{m}\times(\boldsymbol{\sigma}\times\boldsymbol{m})$; and the other is the out-of-plane (OP) field-like (FL) torque[17] $\tau_{\text{FL}} = \tau_{\text{FL}}(\boldsymbol{\sigma}\times\boldsymbol{m})$. Previously many theoretical studies have revealed that the DL torque originates predominantly from the SHE,[18] while the FL torque is dominated by IREE.[15] However, many recent FM thickness- and interface-dependent SOTs efficiency experiments found that the IREE can also significantly contribute to the DL torque with a value comparable to SHE-contribution in some HM/FM systems with strong ISOC. In addition, the interface-related spin memory loss (SML) and spin flow back also play an essential role in the effective SOTs efficiencies. For instance, the SOTs efficiencies can be significantly enhanced by improving interfacial spin transmission efficiency and enhancing IREE via interface engineering, such as inserting ultrathin nonmagnetic metal layer (*e.g.*, Hf,[19] Mo,[20] and Cu[21,22]) between the HM and FM layers, oxygen-induced interface orbital hybridization,[23] alloy,[24] and interfacial H$^+$

†Corresponding author. E-mail: chenlina@njupt.edu.cn
‡Corresponding author. E-mail: tjzhou@hdu.edu.cn
§Corresponding author. E-mail: rhliu@nju.edu.cn

and O^{2-} ion manipulations.[25] Very recently, inserting a magnetic spacer[26,27] between the FM and HM layers has also been proposed as a promising method to improve the effective SOTs efficiencies by selecting suitable magnetic materials to increase ISOC and/or enhance interfacial spin transparency ($T_{\rm int}$).[26] However, the detailed characterization of the ISOC-related interfacial magnetic properties, *e.g.*, interfacial perpendicular magnetic anisotropy (IPMA) energy density,[19] $T_{\rm int}$, two-magnon scattering (TMS) coefficient,[28] the conventional SHE/IREE-induced DL torque efficiency ($\xi_{\rm DL}$) and FL torque efficiency ($\xi_{\rm FL}$) and possible unconventional SOTs of spin currents with OP spin polarization in Pt-based multilayer systems with a strong ISOC still remains a few so far.

In this paper, we study the SOTs efficiencies in the Pt/Co (t)/Py trilayers with a strong ISOC at the Pt/Co interface by spin-torque ferromagnetic resonance (ST-FMR) technique and find a significant enhancement of the $\xi_{\rm DL} = 0.103$ and $\xi_{\rm FL} = -0.017$ in Pt/Co/Py system with an inserting Co layer compared to $\xi_{\rm DL} = 0.051$ and $\xi_{\rm FL} = -0.002$ in the Pt/Py bilayer. The enhancement of SOT efficiencies is related to the IREE-induced additional SOTs at a robust ISOC Pt/Co interface by inserting an ultrathin Co layer between Pt and Py. In addition, these Pt/Co/Py trilayers also exhibit considerable OP spin-polarized SOTs, revealed by the IP angular dependence ST-FMR spectra. The results suggest that the ISOC of the Pt/Co interface plays a vital role in spin transport and SOTs-generation and can be an efficient approach to promote the conventional SOTs efficiency and generate unconventional SOTs for the development of non-volatility, low power, higher speed, and higher endurance spintronic devices.

2. Experiments

The ST-FMR devices consist of the stack structure: Pt(5)/Co($t = 0, 0.2$, 0.3, 0.4, 0.5, 0.75, 1, 1.5, and 2)/Py(4), which are deposited on annealed Al_2O_3 substrate with (0001) orientation by d.c magnetron sputtering at room temperature with Ar sputtering gas pressure of 5.1 mTorr and background base pressure of 2×10^{-8} Torr (1 Torr = 1.33322×10^{2} Pa). The film thickness in parentheses is in nm. A 2-nm-thick MgO is adopted to protect the multilayers from oxidation in air. The films are patterned into a 5 μm×8 μm rectangle stripe with two top electrodes of Au (80) for ST-FMR measurement using the combination of photolithography, electron beam lithography, and ion milling.

3. Results and discussion

Figure 1(a) shows the ST-FMR measurement setup,[29] where a radio-frequency (RF) current ($I_{\rm RF}$) is applied along the longitudinal direction of the stripe by connecting a signal generator, and a dc mixing voltage ($V_{\rm mix}$), generated from rectification among the RF current, SOTs and Oersted field-driven oscillating resistance due to anisotropic magnetoresistance (AMR), is recorded by a lock-in while sweeping an IP external field H. Figure 1(b) shows the representative ST-FMR spectra of Pt(5)/Co(0.4)/Py(4) sample with excitation frequency from 6 GHz to 10 GHz, IP angle $\varphi = 30^\circ$. The obtained $V_{\rm mix}$ can be well fitted with a Lorentzian function[1,23]

$$V_{\rm mix} = V_{\rm s}\frac{\Delta H^2}{\left[(H-H_{\rm res})^2+\Delta H^2\right]} + V_{\rm a}\frac{\Delta H(H-H_{\rm res})}{\left[(H-H_{\rm res})^2+\Delta H^2\right]}, \tag{1}$$

where $V_{\rm s}$, $V_{\rm a}$, ΔH, and $H_{\rm res}$ are the magnitude of the symmetric ($V_{\rm s}$) and antisymmetric ($V_{\rm a}$) Lorentzian components, the linewidth, and resonance field, respectively. The representative $V_{\rm mix}$ data of the Pt(5)/Co(0.4)/Py(4) with $f = 6$ GHz and its fitting curves are illustrated in Fig. 1(c).

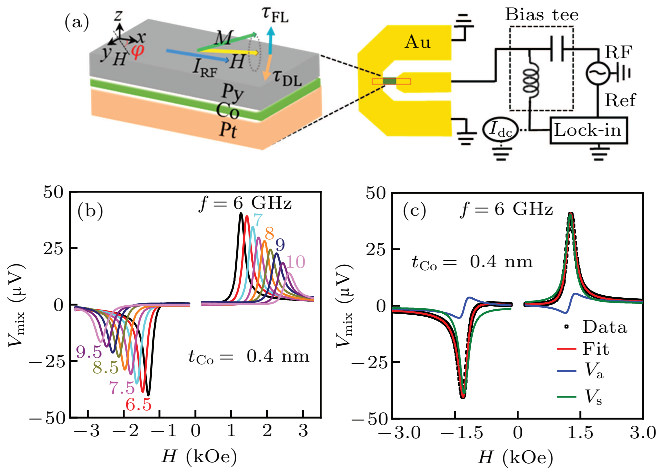

Fig. 1. ST-FMR spectra of Pt/Co/Py. (a) Left: The illustration of the stack structure of multilayer, coordinate system, and SOTs-induced magnetization dynamics in the ST-FMR measurement. Right: the schematic diagram of the ST-FMR setup. (b) ST-FMR spectra of the $V_{\rm mix}$ of the Pt(5)/Co(0.4)/Py(4) sample for frequency f between 6 GHz and 10 GHz increased in 0.5-GHz step at an angle $\varphi = 30^\circ$ between the magnetic field and current direction. (c) Representative ST-FMR spectrum obtained at $f = 6$ GHz and its fitting curves using Eq. (1). $V_{\rm s}$ and $V_{\rm a}$ correspond to the symmetric and antisymmetric Lorentzian components, respectively.

Before discussing the spin torques efficiencies, we first characterize the interfacial properties of the Pt/Co/Py trilayers by quantifying the magnetic anisotropy and effective spin-mixing conductance ($G^{\uparrow\downarrow}_{\rm eff,tot}$) related to the ISOC. The total effective magnetic anisotropy energy density $K_{\rm eff}$ (erg/cm^3) consists of the volume contribution $K_{\rm v}$ and the interfacial $K_{\rm s} = K_{\rm s}^{\rm Pt/Co} + K_{\rm s}^{\rm Co/Py}$ with the following relation:[30,31]

$$K_{\rm eff}t_{\rm FM}^{\rm tot} = K_{\rm v}t_{\rm FM}^{\rm tot} + K_{\rm s}. \tag{2}$$

The effective demagnetization field $4\pi M_{\rm eff} = 4\pi M_{\rm s} - K_{\rm eff}/2\pi M_{\rm s}$ for all studied ST-FMR devices can be obtained by fitting the experimental results of f *versus* $H_{\rm res}$ [Fig. 2(a)] using the Kittel formula[23] $f = (\gamma/2\pi)\sqrt{H_{\rm res}(H_{\rm res}+4\pi M_{\rm eff})}$, where $\gamma/2\pi$ is the gyromagnetic ratio. Figure 2(b) shows the

$4\pi M_{\mathrm{eff}}$ as a function of the inserting Co layer thickness t_{Co}. To quantitatively extract the value of K_{eff}, we also measure the saturation magnetization M_{s} of all samples by vibrating sample magnetometry (VSM), as shown in Fig. 2(c). The M_{s} of all samples can be well fitted by the formula $M_{\mathrm{s}} = \left(M_{\mathrm{s}}^{\mathrm{Py}} t_{\mathrm{Py}} + M_{\mathrm{s}}^{\mathrm{Co}} t_{\mathrm{Co}}\right)/\left(t_{\mathrm{Py}} + t_{\mathrm{Co}}\right)$, with two reasonable parameters $M_{\mathrm{s}}^{\mathrm{Py}} = 707$ emu/cm^3 and $M_{\mathrm{s}}^{\mathrm{Co}} = 1125$ emu/cm^3, consistent with previously reported values[32,33] $M_{\mathrm{s}}^{\mathrm{Py}} = 697$ emu/cm^3 and $M_{\mathrm{s}}^{\mathrm{Co}} = 1084$ emu/cm^3. Therefore, we can determine the K_{eff} from the effective demagnetization field. Figure 2(d) shows that $K_{\mathrm{eff}} t_{\mathrm{FM}}^{\mathrm{tot}}$ for all inserting Co samples exhibits a linear dependence on $t_{\mathrm{FM}}^{\mathrm{tot}}$ except for the Pt/Py bilayer sample, indicating that the interfacial K_{s} is dominated by the Pt/Co and Co/Py interface. From the intercept of the linear fitting with Eq. (2) at $t_{\mathrm{FM}}^{\mathrm{tot}} = 0$, we estimate $K_{\mathrm{s}} = 2.7$ erg/cm^2, comparable with previous reports value.[33,34] Meanwhile, the effective interfacial PMA field $(H_{\perp}) H_{\perp} = 4\pi M_{\mathrm{s}} - 4\pi M_{\mathrm{eff}}$ is also illustrated in the inset of Fig. 2(d), indicating that inserting a thin Co layer between Pt and Py can lead to a large effective OP magnetic anisotropy. The reason is that the 5d-Pt with a strong SOC can modify the perpendicular orbital moments in an adjacent 3d-Co layer via strong interfacial 3d–5d hybridization.[35,36]

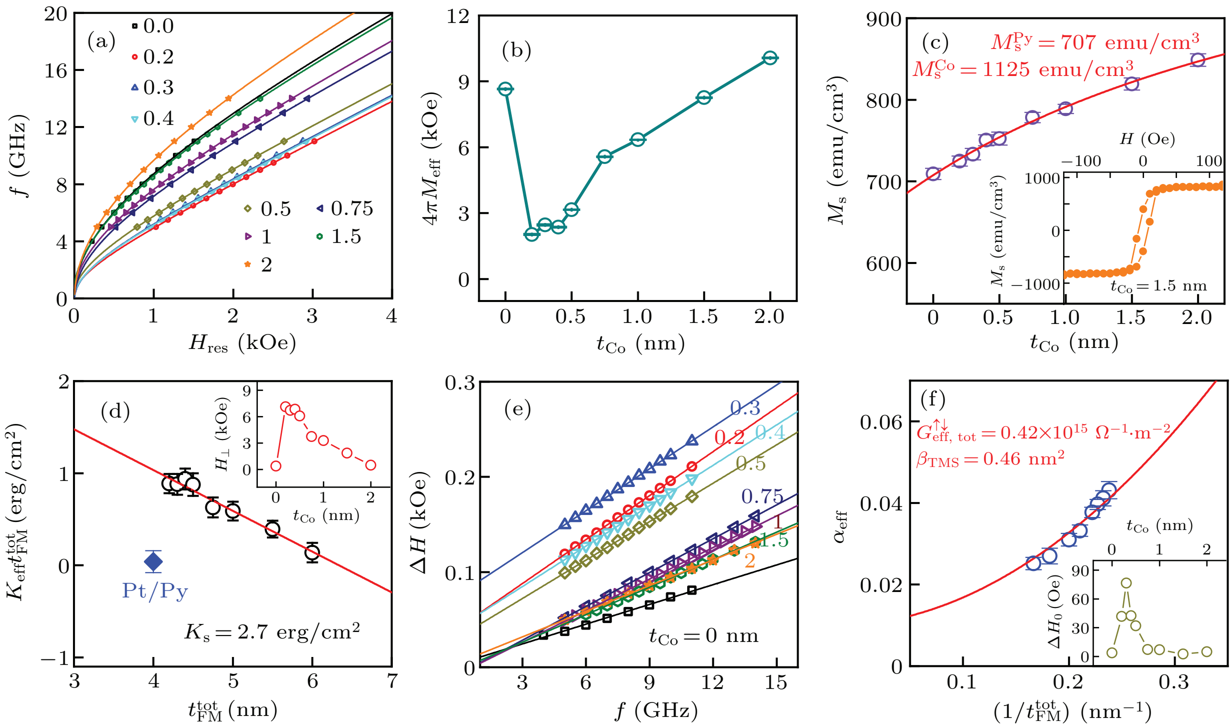

Fig. 2. Thickness-dependent magnetic properties of Py(5)/Co($t_{\mathrm{Co}} = 0$ nm–2 nm)/Py(4) system. (a) Dispersion relation curves between f and H_{res} (symbols) and the corresponding Kittel fittings (solid curves). (b)–(d) Dependence of the effective demagnetization field $4\pi M_{\mathrm{eff}}$ (b), and the saturation magnetization M_{s} (c) and the $H_{\perp}$ (Inset in panel (d)) on the inserting Co layer thickness t_{Co}, and the effective magnetic anisotropy energy in terms of $K_{\mathrm{eff}} t_{\mathrm{FM}}^{\mathrm{tot}}$ (d) on the total FM layer thickness $t_{\mathrm{FM}}^{\mathrm{tot}}$. Inset in panel (c): the representative magnetization curve of $t_{\mathrm{Co}} = 1.5$ nm sample. (e) Linewidth ΔH *versus* resonance frequency f. The solid line is the linear fitting. (f) Damping α_{eff} as a function of $1/t_{\mathrm{FM}}^{\mathrm{tot}}$ (symbols). Inset: dependence of the inhomogeneous line broadening ΔH_0 on the inserting Co layer thickness t_{Co}.

In a magnetic heterostructure HM/FM system, the $G_{\mathrm{eff,tot}}^{\uparrow\downarrow}$ is a key parameter of the indication of spin transmission and SOTs efficiencies, *e.g.*, the T_{int} is proportional to $G_{\mathrm{eff,tot}}^{\uparrow\downarrow}$, and the ξ_{DL} depends on $G_{\mathrm{eff,tot}}^{\uparrow\downarrow}$ in terms of $\xi_{\mathrm{DL}} = T_{\mathrm{int}} \theta_{\mathrm{SH}}$, where θ_{SH} is the intrinsic charge-to-spin convert ratio or spin Hall angle due to SHE/IREE. Therefore, we can get some helpful information about the interface-related spin transparency and spin-mixing conductance from the magnetic damping. The inserting Co layer thickness-dependent effective damping (α_{eff}) can be determined by fitting the experimental results of f *versus* linewidth ΔH [Fig. 2(e)] using[37,38] $\Delta H = (2\pi/\gamma)\,\alpha_{\mathrm{eff}} f + \Delta H_0$ where ΔH_0 is the inhomogeneous linewidth. ΔH_0 exhibits a significant enhancement for the samples by inserting Co thickness $t_{\mathrm{Co}} = 0.2$ nm–0.5 nm [Inset of Fig. 2(f)], which is related to the inhomogeneity of interfacial magnetic anisotropy and magnetic properties caused by the discussed ISOC of Pt/Co above. The extracted α_{eff} as a function of the total thickness of the FM layer is shown in Fig. 2(f). As we know, besides the FM layer thickness-independent intrinsic Gilbert damping (α_{int}), the α_{eff} contains additional two main contributions: $G_{\mathrm{eff,tot}}^{\uparrow\downarrow}$ related to spin pumping and TMS due to ISOC and magnetic defects at interfaces. The total α_{eff} is given approximately[28,39]

$$\alpha_{\mathrm{eff}} = \alpha_{\mathrm{int}} + G_{\mathrm{eff,tot}}^{\uparrow\downarrow} \frac{g\mu_{\mathrm{B}} h}{4\pi M_{\mathrm{s}} e^2} \frac{1}{t_{\mathrm{FM}}^{\mathrm{tot}}} + \beta_{\mathrm{TMS}} \frac{1}{t_{\mathrm{FM}}^{\mathrm{tot}2}}, \tag{3}$$

where g is the Lande factor, μ_{B} is the Bohr magnetron, and

h is the Planck's constant. The second term is related to the spin currents loss via spin pumping into the Pt layer and being absorbed due to SML at the Pt/Co and Co/Py interfaces,[39] and the third term is the contribution from the TMS process, where the TMS coefficient β_{TMS} depends on both $(2K_{\mathrm{s}}/M_{\mathrm{s}})^2$ and the density of magnetic defect at the interfaces. Fitting the dependence of α_{eff} on $1/t_{\mathrm{FM}}^{\mathrm{tot}}$ in Fig. 2(f) by using Eq. (3), we determine the $\alpha_{\mathrm{int}} = 0.010$ of FM layer and the $G_{\mathrm{eff,tot}}^{\uparrow\downarrow} = 0.42 \times 10^{15}\ \Omega^{-1}\cdot\mathrm{m}^{-2}$, which is comparable with the previously reported value $G_{\mathrm{eff,tot}}^{\uparrow\downarrow} = 0.31 \times 10^{15}\ \Omega^{-1}\cdot\mathrm{m}^{-2}$ of the Pt/Co bilayer,[28,39] suggesting the Pt/Co interface dominates the interfacial SOTs efficiencies and T_{int}. Additionally, we also find that the TMS is nonnegligible and the fitting parameter $\beta_{\mathrm{TMS}} = 0.46\ \mathrm{nm}^2$ indicates that the Pt/Co/Py trilayer has a much stronger TMS than the Pt/Py bilayer due to the strong ISOC-induced IPMA and interfacial scattering.

To further examine how the above Pt/Co interfacial characteristics of K_{s}, $G_{\mathrm{eff,tot}}^{\uparrow\downarrow}$ and the coefficient β_{TMS} are reflected in the ξ_{DL} and ξ_{FL}, we adopt two methods of lineshape analysis ($V_{\mathrm{s}}/V_{\mathrm{a}}$) and linewidth modulation (LWM) to quantify the SOTs via the ST-FMR spectra. Based on the previous reports[1,23] of the HM/FM bilayer system with the conventional SHE/IREE, the V_{s} and V_{a} components originate from the OP DL effective field H_{DL} and IP Oersted field H_{Oe} and/or FL effective field H_{FL}, respectively. Therefore, the spin-torque efficiency (ξ_{FMR}) can be estimated by the $V_{\mathrm{s}}/V_{\mathrm{a}}$ ratio as[33,34,40]

$$\xi_{\mathrm{FMR}} = \frac{V_{\mathrm{s}}}{V_{\mathrm{a}}}\frac{e4\pi M_{\mathrm{s}} t_{\mathrm{FM}}^{\mathrm{tot}} t_{\mathrm{HM}}}{\hbar}\sqrt{1+4\pi M_{\mathrm{eff}}/H_{\mathrm{res}}}, \tag{4}$$

where t_{HM} and $t_{\mathrm{FM}}^{\mathrm{tot}}$ represent thicknesses of the Pt layer and the total FM layer, respectively. ξ_{FMR} depends on $t_{\mathrm{FM}}^{\mathrm{tot}}$ because H_{FL} is inversely proportional to the FM layer thickness in terms of $H_{\mathrm{FL}} \propto \xi_{\mathrm{FL}}/t_{\mathrm{FM}}^{\mathrm{tot}}$ and H_{Oe} is independent of $t_{\mathrm{FM}}^{\mathrm{tot}}$. Furthermore, ξ_{FMR} can be divided into the ξ_{DL} and ξ_{FL} as the following formula:

$$\frac{1}{\xi_{\mathrm{FMR}}} = \frac{1}{\xi_{\mathrm{DL}}}\left(1 + \frac{\hbar}{e}\frac{\xi_{\mathrm{FL}}}{4\pi M_{\mathrm{s}} t_{\mathrm{FM}}^{\mathrm{tot}} t_{\mathrm{HM}}}\right), \tag{5}$$

where e is the electronic charge, $\hbar$ is the reduced Planck's constant. To disentangle SOTs efficiencies, we need to get thickness-dependent ξ_{FMR} by varying the thickness of the inserting Co layer. Figure 3(a) shows the normalized ST-FMR spectra voltage of all studied samples with $t_{\mathrm{Co}} = 0$ nm–2 nm at $f = 6$ GHz. The V_{s} and V_{a} components can be determined by fitting ST-FMR spectra using a Lorentzian function Eq. (1). According to Eq. (4), we calculate the ξ_{FMR} of all samples as a function of the intercalation Co thickness t_{Co}, as shown in Fig. 3(b). Then, the $\xi_{\mathrm{DL}} = 0.103$ and $\xi_{\mathrm{FL}} = -0.017$ are determined by using a linear function Eq. (5) to fit $1/\xi_{\mathrm{FMR}}$ *versus* $1/t_{\mathrm{FM}}^{\mathrm{tot}}$ data [Fig. 3(c)]. The obtained values are consistent with the previous reports in the pure Pt/Co bilayer systems.[33]

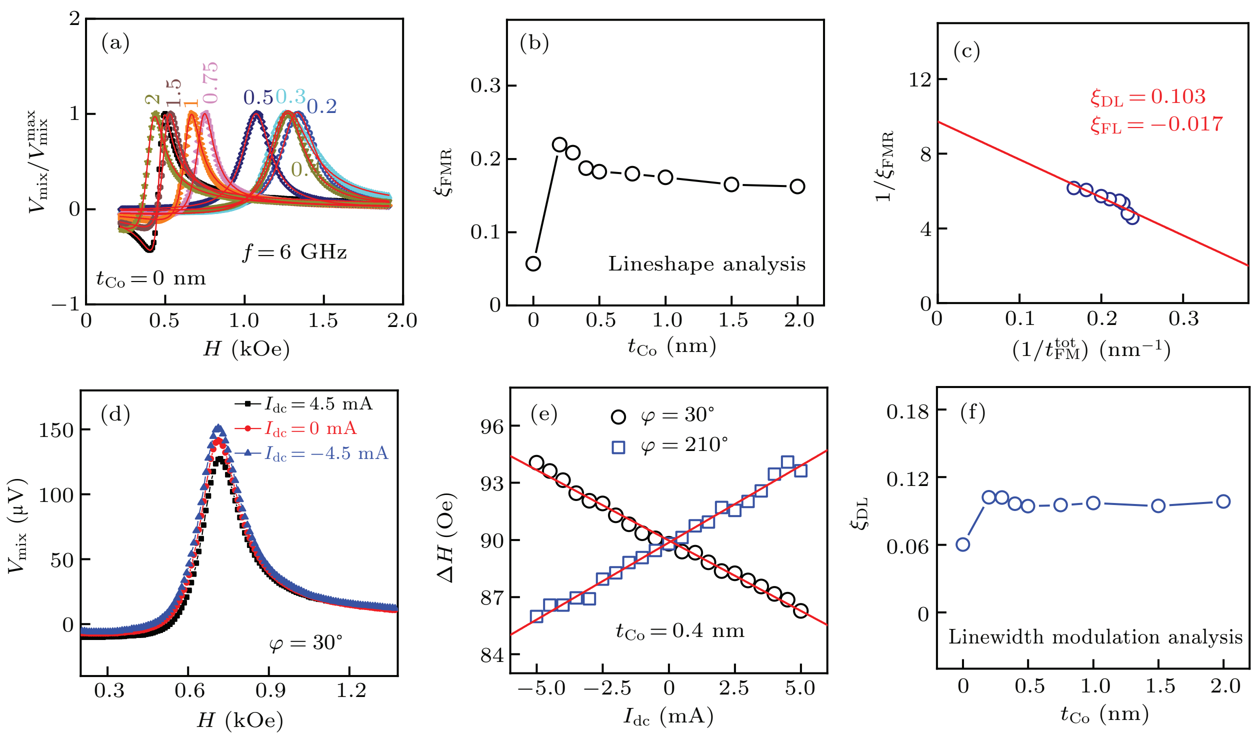

Fig. 3. Thickness-dependent ξ_{DL} and ξ_{FL}. (a) The normalized ST-FMR spectra voltage of all studied samples with $t_{\mathrm{Co}} = 0$ nm–2 nm at $f = 6$ GHz (symbols) and the fitting results using Eq. (1) (solid lines). (b) The ξ_{FMR} of all films as a function of the interlayer Co thickness evaluated by the ratio $V_{\mathrm{s}}/V_{\mathrm{a}}$. (c) The relation of $1/\xi_{\mathrm{FMR}}$ *versus* $1/t_{\mathrm{FM}}^{\mathrm{tot}}$ and its linear fitting using Eq. (5) in the text. (d) ST-FMR spectra at different dc bias currents I_{dc} with an IP angle $\varphi = 30^\circ$ for the $t_{\mathrm{Co}} = 0.4$ nm sample. (e) Linewidth as a function of applied dc bias current I_{dc} in the case of IP angle $\varphi = 30^\circ$ (black circles) and $\varphi = 210^\circ$ (red squares) for the $t_{\mathrm{Co}} = 0.4$ nm sample. The solid red lines are the linear fittings. (f) The inserting Co layer thickness t_{Co} dependence of ξ_{DL} determined by the LWM method.

To further confirm the validity of the above determined ξ_{DL}, we also adopt an alternative approach to quantify ξ_{DL} based on the LWM by dc current-induced DL SOT acting on the FM layer.[23] ξ_{DL} can be extracted through dc current-dependent linewidth ΔH measurements by the following formula:[1,23]

$$\xi_{\mathrm{DL}}=\frac{\Delta H/I_{\mathrm{dc}}}{\frac{2\pi f}{\gamma}\frac{\sin\varphi}{(H_{\mathrm{res}}+2\pi M_{\mathrm{eff}})4\pi M_{\mathrm{s}}t_{\mathrm{FM}}^{\mathrm{tot}}}\frac{\hbar}{2e}}\frac{R_{\mathrm{FM}}+R_{\mathrm{HM}}}{R_{\mathrm{FM}}}A_{\mathrm{c}},\quad(6)$$

where R_{FM} and R_{HM} are the resistance of the total FM and Pt layers, respectively, and A_{c} is the cross-sectional area of the Pt layer. Figure 3(d) shows the representative ST-FMR spectra at different dc bias currents I_{dc} at an IP angle $\varphi=30^{\circ}$. The extracted current-dependent linewidth ΔH at two IP angles $\varphi=30^{\circ}$ and 210° for $t_{\mathrm{Co}}=0.4$ nm sample at $f=4$ GHz were shown in Fig. 3(e). The obtained ξ_{DL} using Eq. (6) exhibits a nearly constant value of $\xi_{\mathrm{DL}}\approx0.10$ for all inserting Co samples [Fig. 3(f)], closing to 0.103 obtained by the above $V_{\mathrm{s}}/V_{\mathrm{a}}$ method. These $\xi_{\mathrm{DL}}=0.103$ and $\xi_{\mathrm{FL}}=-0.017$ are significantly larger than $\xi_{\mathrm{DL}}=0.051$ and $\xi_{\mathrm{FL}}=-0.002$ in the Pt/Py bilayer,[1] indicating that the ISOC at the interface Pt/Co plays a vital role in both generating SOTs and spin transmission discussed above.

Since the ST-FMR voltage signal V_{mix} of our studied microscale device is mainly contributed by the rectification of I_{RF} and I_{RF} induced periodic magnetoresistance due to the AMR effect, and with a negligible inverse SHE voltage due to spin pumping, the IP angular dependence of the V_{a} and V_{s} components of V_{mix} is related to the combination of the angular dependences of the AMR and the generated spin currents and the current-induced Oersted field. The AMR exhibits the sinusoidal dependence on magnetization with a period of 180°, $R_{\mathrm{AMR}}\propto\sin2\varphi$. Considering the generated spin currents with all possible spin polarizations, we can derive the general formula for describing IP angular-dependent V_{a} and V_{s} of ST-FMR voltage as follows:[41,42]

$$V_{\mathrm{a}}=(V_{\mathrm{a},y}\cos\varphi+V_{\mathrm{a},z}+V_{\mathrm{a},x}\sin\varphi)\sin2\varphi,\quad(7)$$

$$V_{\mathrm{s}}=(V_{\mathrm{s},y}\cos\varphi+V_{\mathrm{s},z}+V_{\mathrm{s},x}\sin\varphi)\sin2\varphi.\quad(8)$$

The $V_{\mathrm{a},y}$ corresponds to the OP torque arising from current-induced IP Oersted field and the effective field due to the generated spin currents with spin polarization (σ_y) via SHE/IREE, and $V_{\mathrm{s},y}$ is attributed to the SHE/IREE-induced IP DL torque. The $V_{\mathrm{a},z}$ and $V_{\mathrm{s},z}$ originate from the OP DL torque $\tau_{\perp,\mathrm{DL}}$ and the IP FL torque $\tau_{\parallel,\mathrm{FL}}$ generated by the spin currents with OP spin polarization ($\boldsymbol{\sigma}_z$), respectively. The $V_{\mathrm{a},x}$ and $V_{\mathrm{s},x}$ are correlated with the OP FL torque and IP DL torque due to the spin currents with spin polarization ($\boldsymbol{\sigma}_x$) along the charge current direction (x direction).

To explore the possible existence of unconventional SOTs arising from the spin currents with $\boldsymbol{\sigma}_z$ and $\boldsymbol{\sigma}_x$ except for conventional $\boldsymbol{\sigma}_y$, we perform the IP angular dependence of the ST-FMR spectra. Figures 4(a) and 4(b) show the IP angular dependent V_{a} and V_{s} and their fitting curves using Eqs. (7) and (8) for the representative sample of Pt(5)/Co(0.4)/Py(4) under $f=6$ GHz. The fitting parameters $V_{\mathrm{a},x}$ and $V_{\mathrm{s},x}$ have the negligible small value compared to $V_{\mathrm{a},y}$, indicating that the generated spin currents with σ_x are negligible. However, there exists a considerable value for $V_{\mathrm{a},z}$ and $V_{\mathrm{s},z}$, which can be used to quantify the strength of $\tau_{\perp,\mathrm{DL}}$ and $\tau_{\parallel,\mathrm{FL}}$ by directly comparing $V_{\mathrm{a},z}$ and $V_{\mathrm{s},z}$ to $V_{\mathrm{a},y}$ because $V_{\mathrm{a},y}$ is mainly proportional to I_{RF}-induced Oersted field. Therefore, $V_{\mathrm{a},z}/V_{\mathrm{a},y}$ and $V_{\mathrm{s},z}/V_{\mathrm{a},y}$ represent the strengths of the OP DL and IP FL torques exerted by the generated spin currents with $\boldsymbol{\sigma}_z$. Figure 4(c) shows that $|V_{\mathrm{a},z}/V_{\mathrm{a},y}|$ and $|V_{\mathrm{s},z}/V_{\mathrm{a},y}|$ as a function of the inserting Co layer thickness for all studied samples exhibit a maximum at $t_{\mathrm{Co}}=0.4$ nm. At the same thickness, the $H_{\perp}$ also exhibits the maximum. The generated spin currents with the OP spin polarization are proportional to the $H_{\perp}$, suggesting that the strong 3d-Co and 5d-Pt orbital hybridization at the Pt/Co interface can generate a considerable OP DL torque $\tau_{\perp,\mathrm{DL}}$ to facilitate current-induced magnetization switching in the HM/FM systems without needing an assistant field.[43] However, in the previous theory reports,[44,45] several proposed possible mechanisms, *e.g.*, spin swapping,[44] spin–orbit precession,[46] and/or spin anomalous Hall effect,[47,48] can generate these spin currents with σ_z, warranting further theoretical and experimental studies of the behind mechanism of interface dependence of this σ_z-spin currents.

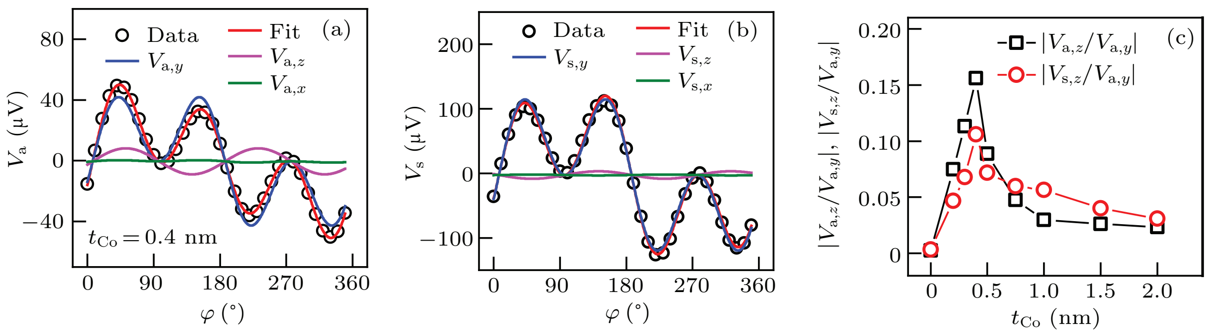

Fig. 4. Unconventional SOTs with OP spin polarization in Pt/Co ($t_{\mathrm{Co}}=0.2$ nm–2 nm)/Py. (a)–(b) IP angular-dependent V_{a} (a) and V_{s} (b) of ST-FMR voltage signal for a representative Pt(5)/Co(0.4)/Py(4) sample at $f=6$ GHz can be well fitted by the combination of three terms: $V_y\sin2\varphi\cos\varphi$ (blue line), $V_z\sin2\varphi$ (pink line), and $V_x\sin2\varphi\sin\varphi$ (green line). (c) The absolute value of $V_{\mathrm{a},z}/V_{\mathrm{a},y}$ and $V_{\mathrm{s},z}/V_{\mathrm{a},y}$ as a function of t_{Co}.

4. Conclusion

In summary, we systematically investigate the ISOC phenomena (IPMA coefficient $G_{\text{eff,tot}}^{\uparrow\downarrow}$, TMS coefficient, and SOTs efficiencies) in Pt/Co/Py trilayers system by performing the Co interlayer thickness dependence and IP angular dependence of ST-FMR spectra measurements. Compare to SHE-induced $\xi_{\text{DL}} = 0.051$ and $\xi_{\text{FL}} = -0.002$ in the Pt/Py bilayer, we experimentally demonstrated that the Pt/Co/Py trilayer has a significant enhancement in SHE-generated IP transverse polarization $\boldsymbol{\sigma}_y$ spin current torques $\xi_{\text{DL}} = 0.103$ and $\xi_{\text{FL}} = -0.017$. An enhancement of 80% in the ξ_{DL} is primarily contributed to the additional IREE due to the strong ISOC between Co-3d and Pt-5d orbitals at the Pt/Co interface via bringing in an ultrathin Co interlayer, which is confirmed by ISOC-related spin properties characteristics, such as a large IPMA energy density $K_s = 2.7$ erg/cm^2, a strong TMS coefficient $\beta_{\text{TMS}} = 0.46$ nm^2, and a moderate effective $G_{\text{eff,tot}}^{\uparrow\downarrow} = 0.42 \times 10^{15}\ \Omega^{-1} \cdot \text{m}^{-2}$. Additionally, a considerable $\boldsymbol{\sigma}_z$-spin currents with a maximum at $t_{\text{Co}} = 0.4$ nm, which are proportional to the $H_{\perp}$, suggesting that the generated $\boldsymbol{\sigma}_z$-spin currents are correlated to the effective M_z component. Our results suggest that the interfacial magnetic properties, spin current generation, and spin transport in the hybrid heterostructure thin film can be effectively manipulated by tailoring their interfaces.

Acknowledgments

Project supported by the National Natural Science Foundation of China (Grant Nos. 11774150, 12074178, 11874135, and 12004171), the Applied Basic Research Programs of the Science and Technology Commission Foundation of Jiangsu Province, China (Grant No. BK20200309), the Open Research Fund of Jiangsu Provincial Key Laboratory for Nanotechnology, Key Research and Development Program of Zhejiang Province, China (Grant No. 2021C01039), and the Scientific Foundation of Nanjing University of Posts and Telecommunications (Grant No. NY220164).

References

[1] Liu L Q, Moriyama T, Ralph D C and Buhrman R A 2011 *Phys. Rev. Lett.* **106** 036601
[2] Liu R H, Lim W L and Urazhdin S 2014 *Phys. Rev. B* **89** 220409
[3] Wang M, Guo Q, Xu X, Zhang Z, Ren Z, Zhu L, Meng K, Chen J, Wu Y, Miao J and Jiang Y 2020 *Adv. Electron. Mater.* **6** 2000229
[4] Zhu L, Xu X, Wang M, Meng K, Wu Y, Chen J, Miao J and Jiang Y 2020 *Appl. Phys. Lett.* **117** 112401
[5] Feng X, Zhang Q, Zhang H, Zhang Y, Rui, Lu B, Cao J and Fan X 2019 *Chin. Phys. B* **28** 107105
[6] Li S and Zhu T 2020 *Chin. Phys. B* **29** 087102
[7] Liu J, Wang Z, Xu T, Zhou H, Zhao L, Je S G, Im M Y, Fang L and Jiang W 2022 *Chin. Phys. Lett.* **39** 017501
[8] Zheng Z, Zhang Y, Zhu D, Zhang K, Feng X, He Y, Chen L, Zhang Z, Liu D, Zhang Y, Amiri P K and Zhao W 2020 *Chin. Phys. B* **29** 078505
[9] Wang M, Cai W, Zhu D, Wang Z, Kan J, Zhao Z, Cao K, Wang Z, Zhang Y, Zhang T, Park C, Wang J P, Fert A and Zhao W 2018 *Nat. Electron.* **1** 582
[10] Chen L, Urazhdin S, Du Y W and Liu R H 2019 *Phys. Rev. Appl.* **11** 064038
[11] Li L, Chen L, Liu R and Du Y 2020 *Chin. Phys. B* **29** 117102
[12] Jiang W, Chen L, Zhou K, Li L, Fu Q, Du Y and Liu R H 2019 *Appl. Phys. Lett.* **115** 192403
[13] Chen Y B, Yang X K, Yan T, Wei B, Cui H Q, Li C, Liu J H, Song M X and Cai L 2020 *Chin. Phys. Lett.* **37** 078501
[14] Zheng C, Chen H H, Zhang X, Zhang Z and Liu Y 2019 *Chin. Phys. B* **28** 037503
[15] Zhao Y, Yang G, Dong B, Wang S, Wang C, Sun Y, Zhang J and Yu G 2016 *Chin. Phys. B* **25** 077501
[16] Ye X G, Zhu P F, Xu W Z, Shang N, Liu K and Liao Z M 2022 *Chin. Phys. Lett.* **39** 037303
[17] Amin V P and Stiles M D 2016 *Phys. Rev. B* **94** 104419
[18] Hirsch J E 1999 *Phys. Rev. Lett.* **83** 1834
[19] Pai C F, Nguyen M H, Belvin C, Vilela-Leão L H, Ralph D C and Buhrman R A 2014 *Appl. Phys. Lett.* **104** 082407
[20] Gweon H K, Lee K J and Lim S H 2019 *Appl. Phys. Lett.* **115** 122405
[21] Ni L, Chen Z, Lu X, Yan Y, Jin L, Zhou J, Yue W, Zhang Z, Zhang L, Wang W, Wang Y L, Ruan X, Liu W, He L, Zhang R, Zhang H, Liu B, Liu R, Meng H and Xu Y 2020 *Appl. Phys. Lett.* **117** 112402
[22] Liu F, Zhou C, Tang R, Chai G and Jiang C 2021 *J. Magn. Magn. Mater.* **540** 168462
[23] Yang L, Fei Y, Zhou K, Chen L, Fu Q, Li L, Yan C, Li H, Du Y and Liu R 2021 *Appl. Phys. Lett.* **118** 032405
[24] He C, Chen Q, Shen S, Wei J, Xu H, Zhao Y, Yu G and Wang S 2021 *Chin. Phys. B* **30** 037503
[25] Peng W L, Zhang J Y, Feng G N, Xu X L, Yang C, Jia Y L and Yu G H 2019 *Appl. Phys. Lett.* **115** 092402
[26] Zhang W, Han W, Jiang X, Yang S H and Stuart Parkin S P 2015 *Nat. Phys.* **11** 496
[27] Shu X, Zhou J, Liu L, Lin W, Zhou C, Chen S, Xie Q, Ren L, Yu X, Yang H and Chen J 2020 *Phys. Rev. Appl.* **14** 054056
[28] Zhu L, Zhu L, Ralph D C and Buhrman R A 2020 *Phys. Rev. Appl.* **13** 034038
[29] Wang Y, Ramaswamy R and Yang H 2018 *J. Phys. D: Appl. Phys.* **51** 273002
[30] Johnson M T, Bloemen P J H, Aden Broeder F J and de Vries J J 1996 *Rep. Prog. Phys.* **59** 1409
[31] Yang M, Lu X, Liu B, Ruan X, Zhang J, Zhang X, Huang D, Wu J, Du J, Liu B, Meng H, He L and Xu Y 2020 *Chin. Phys. Lett.* **37** 107502
[32] Wang Y, Deorani P, Qiu X, Kwon J H and Yang H 2014 *Appl. Phys. Lett.* **105** 152412
[33] Pai C F, Ou Y, Vilela-Leão L H, Ralph D C and Buhrman R A 2015 *Phys. Rev. B* **92** 064426
[34] Moriya H, Musha A and Ando K 2021 *Appl. Phys. Express* **14** 063001
[35] Nakajima N K T, Shidara T, Miyauchi H, Fukutani H, Fujimori A, Iio K, Katayama T, Nyvlt M and Suzuki Y 1998 *Phys. Rev. Lett.* **81** 5229
[36] Li R, Li Y, Sheng Y and Wang K 2021 *Chin. Phys. B* **30** 028506
[37] Wang J, Tu H Q, Liang J, Zhai Y, Liu R B, Yuan Y, Huang L A, Liu T Y, Liu B, Meng H, You B, Zhang W, Xu Y B and Du J 2020 *Chin. Phys. B* **29** 107503
[38] Fu Q, Zhou K, Chen L, Xu Y, Zhou T, Wang D, Chi K, Meng H, Liu B, Liu R and Du Y 2020 *Chin. Phys. Lett.* **37** 117501
[39] Zhu L, Ralph D C and Buhrman R A 2019 *Phys. Rev. Lett.* **123** 057203
[40] Hayashi H, Musha A, Sakimura H and Ando K 2021 *Phys. Rev. Res.* **3** 013042
[41] Chen Q, Lv W, Li S, Lv W, Cai J, Zhu Y, Wang J, Li R, Zhang B and Zeng Z 2021 *Chin. Phys. B* **30** 097506
[42] Wang W, Fu Q, Zhou K, Chen L, Yang L, Li Z, Tao Z, Yan C, Liang L, Zhan X, Du Y and Liu R 2022 *Phys. Rev. Appl.* **17** 034026
[43] Chen X, Shi S, Shi G, Fan X, Song C, Zhou X, Bai H, Liao L, Zhou Y, Zhang H, Li A, Chen Y, Han X, Jiang S, Zhu Z, Wu H, Wang X, Xue D, Yang H and Pan F 2021 *Nat. Mater.* **20** 800
[44] Amin V P, Zemen J and Stiles M D 2018 *Phys. Rev. Lett.* **121** 136805
[45] Davidson A, Amin V P, Aljuaid W S, Haney P M and Fan X 2020 *Phys. Lett. A* **384** 126228
[46] Humphries A M, Wang T, Edwards E R J, Allen S R, Shaw J M, Nembach H T, Xiao J Q, Silva T J and Fan X 2017 *Nat. Commun.* **8** 911
[47] Iihama S, Taniguchi T, Yakushiji K, Fukushima A, Shiota Y, Tsunegi S, Hiramatsu R, Yuasa S, Suzuki Y and Kubota H 2018 *Nat. Electron.* **1** 120
[48] Cespedes-Berrocal D, Damas H, Petit-Watelot S, Maccariello D, Tang P, Arriola-Cordova A, Vallobra P, Xu Y, Bello J L, Martin E, Migot S, Ghanbaja J, Zhang S, Hehn M, Mangin S, Panagopoulos C, Cros V, Fert A and Rojas-Sanchez J C 2021 *Adv. Mater.* **33** 2007047